MATERIALS SCIENCE

Bubbles in superfluid helium containing six and eight electrons: Soft, quantum nanomaterial

Neha Yadav[1], Prosenjit Sen[2], Ambarish Ghosh[1,2]*

The role of quantum fluctuations in the self-assembly of soft materials is relatively unexplored, which could be important in the development of next-generation quantum materials. Here, we report two species of nanometer-sized bubbles in liquid helium-4 that contain six and eight electrons, forming a versatile, platform to study self-assembly at the intersection of classical and quantum worlds. These objects are formed through subtle interplay of the short-range electron-helium repulsion and easy deformability of the bulk liquid. We identify these nanometric bubbles in superfluid helium using cavitation threshold spectroscopy, visualize their decoration of quantized vortex lines, and study their creation through multiple methods. The objects were found to be stable for at least 15 milliseconds at 1.5 kelvin and can therefore allow fundamental studies of few-body quantum interactions under soft confinements.

INTRODUCTION

Arrangement of interacting entities under different physical conditions and geometrical constraints plays crucial role in determining the structure and properties of self-organized systems. For most soft materials, the assembly (*1*) can be understood within the framework of classical physics, while quantum effects are readily evident in molecular systems on solid substrates (*2*–*4*). Considering entities not only interact with each other but also interact with the environment; it is natural to wonder how they self-assemble under flexible (soft) confinements. In this regard, organization of electrons within liquid helium is of great interest (see Fig. 1A) (*5*), where surface deformations of a low surface tension liquid can be balanced by the short-range quantum mechanical repulsion of electrons to the helium atoms. In the simplest case, this results in the formation of nanometer-sized bubbles in liquid helium (^{4}He) containing single electrons. The stability of the single-electron bubble (SEB) (*6*, *7*) at zero pressure is governed by the inward pressure due to surface curvature ($P = 2\sigma/R$) balanced by the outward pressure due to the electronic confinement ($P = \hbar^2/16\pi m R^5$), where h, m, σ, and R are Planck's constant, mass of a free electron, surface tension of liquid helium, and radius of the SEB, respectively. The equilibrium radius $R \sim 2$ nm can be further tuned by applying pressure to the liquid.

While cavities containing single electrons (SEBs) have been studied extensively in the past, here, we report the first experimental observation of few-electron bubbles (FEBs): nanometer-sized cavities within liquid helium containing multiple electrons, stabilized by quantum confinement and surface curvature, with additional effects due to interelectron electrostatic, quantum exchange, and correlation interactions. The electrons are pushed to the cavity walls due to electrostatic interactions and finding that their equilibrium configuration closely resembles the Thomson problem (*8*): determining the equilibrium configuration of N charges constrained to move on the surface of a sphere. A crucial additional aspect of the system discussed here is brought about by the flexible and quantum-confined nature (*9*) of the constraint condition, arising because of low surface tension of liquid helium. This results in highly nonspherical shapes, such as the 3EB (FEB with three electrons) shown in Fig. 1B. The equilibrium shape and electronic configuration are nontrivial, with numerical predictions (*10*–*12*) shown in Fig. 1 (B and C) for FEBs of different numbers (Z) of electrons. The sizes vary with applied pressure and Z, e.g., the largest dimension of the 6EB at zero pressure is ~10 nm. As shown in Fig. 1C, calculation predicts FEBs with $Z = 3, 6, 8, 12$ to be stable in a certain range of pressure. Note that it was possible to find multiple stable configurations for a certain FEB, e.g., the electrons in 8EB can exist in cubic, as well as rotated square symmetries. These calculations suggest that FEBs with 6, 8, and 12 electrons could be stable at zero pressure and therefore observable under standard experimental conditions. The lower range of the pressure, e.g., −0.6 bars for 6EB, corresponds to the critical condition for cavitation, where the bubbles become hydrodynamically unstable and grow to macroscopic sizes. Our experimental method is based on measurement of the critical pressure of cavitation, which depends on the number of electrons within a certain FEB. For calibration, we consider the critical pressure for cavitation of the SEB, given by $P_e = -2.12$ bars.

RESULTS

Imaging FEBs with a planar transducer

The experimental setup is schematically shown in Fig. 2A. A negative voltage pulse was applied to the sharp tungsten tip (amplitude, −1 to −2 kV; duration, 0.2 to 0.6 ms) to generate a discharge (details in description of Fig. 3 and section S1) above the surface. Negative potentials applied to the top ring and confinement cylinders ensure a dense layer of electrons confined above the surface. The planar ultrasonic transducer was driven at 1 MHz for 200 μs, which generated a pressure wave in superfluid ^{4}He at 1.5 K of amplitude proportional to the transducer peak to peak voltage, V_T. Beyond a certain $V_T \sim 140$ V, cavitation events could be detected where the bubbles would grow to sizes (*13*) larger than 10 μm and thereby imaged using a high-speed camera running at 10,000 frames/s (fps) (see movie S1). The number of events occurring in the bulk (away from transducer surface) averaged over 200 trials is plotted as a function of V_T in Fig. 2B, which shows two distinct regimes. These correspond to cavitation nucleated on two distinct objects, marked with

[1]Department of Physics, Indian Institute of Science, Bangalore 560012, India. [2]Centre for Nano Science and Engineering, Indian Institute of Science, Bangalore 560012, India.
*Corresponding author. Email: ambarish@iisc.ac.in

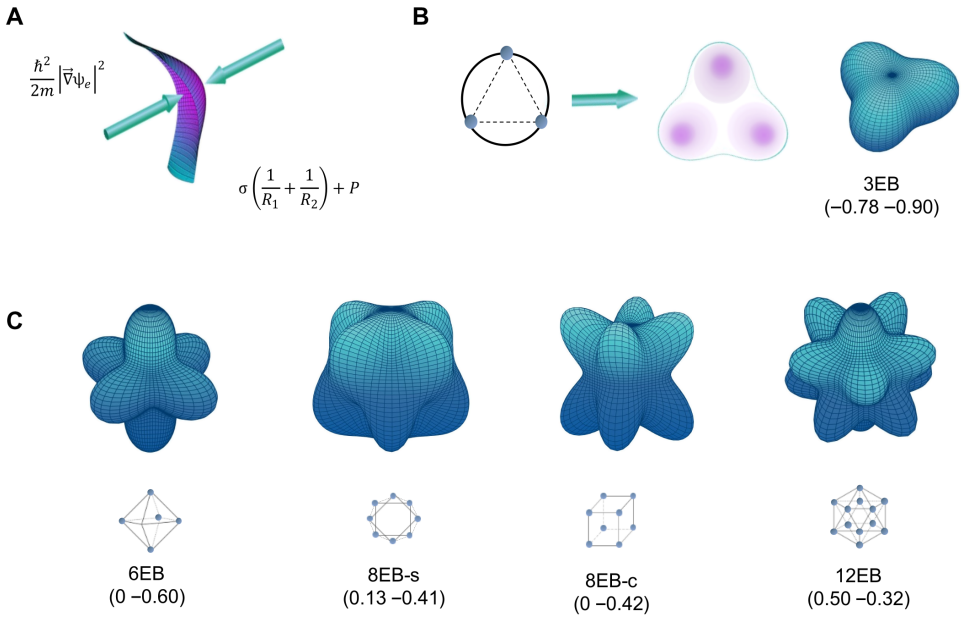

Fig. 1. Structure of FEBs. (**A**) Interplay of quantum confinement balanced by surface curvature and applied pressure, determining the configuration of electrons interacting with liquid helium. (**B**) Formation of a 3EB where the three electrons interact electrostatically and equilibrate within a deformed cavity. (**C**) Calculated shapes (not to scale) and spatial arrangement of the electrons for FEBs (*10*, *11*). Also shown is the range of pressures, where the respective FEBs are stable against small fluctuations.

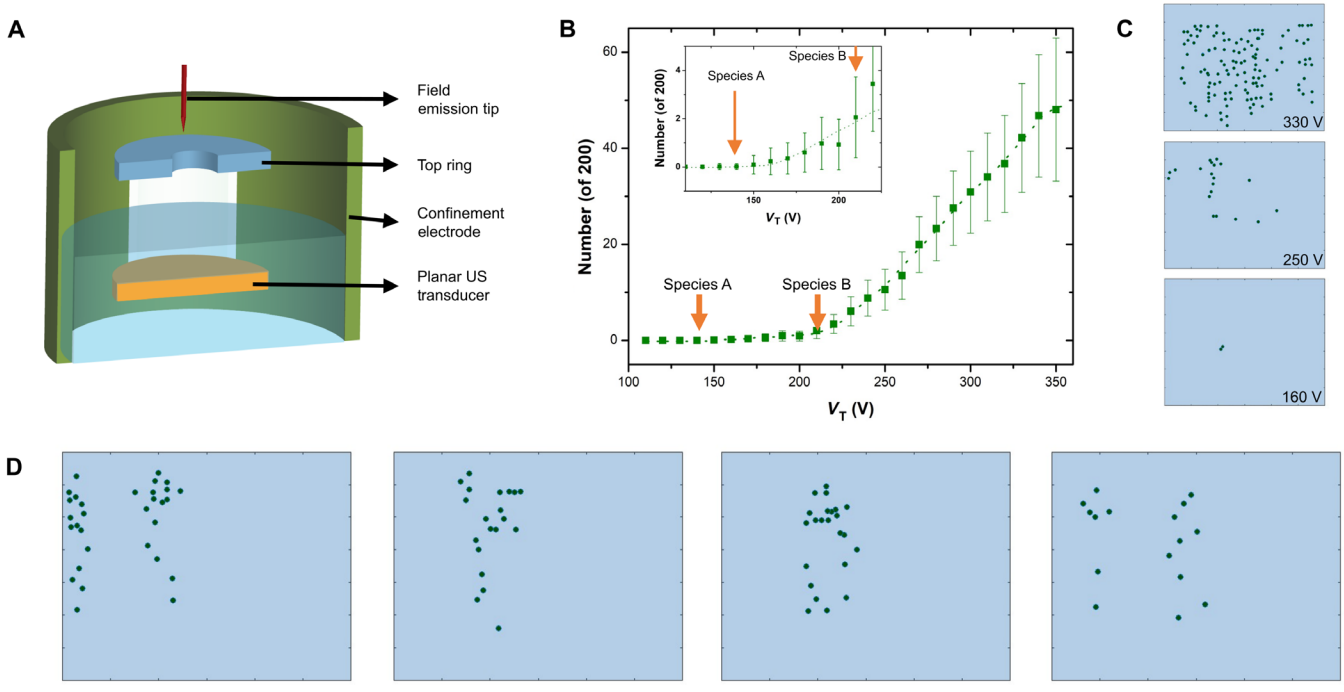

Fig. 2. Imaging and identifying FEBs. (**A**) Experimental setup: Voltage pulse applied to a sharp tungsten tip produced a discharge above the liquid surface. Potential applied to metal rings and cylinders, denoted as top ring and confinement electrodes respectively, ensured that the surface was highly charged. A planar ultrasonic (US) transducer was used to generate a pressure wave that induced cavitation on the FEBs. (**B**) Number of FEBs observed as a function of voltage applied to the ultrasonic transducer, averaged over 200 trials. Two distinct thresholds can be observed suggesting two different species (shown by arrows) of FEBs (see inset). (**C**) Example cases of locations of cavitation events (therefore, FEB positions) within the experimental volume at specified transducer voltages. (**D**) Snapshots of the experimental chamber of observation window (5 mm by 3.5 mm), corresponding to a transducer voltage of 250 V showing FEBs to be located along curved paths inside the liquid, suggesting that they were trapped on quantized vortex lines.

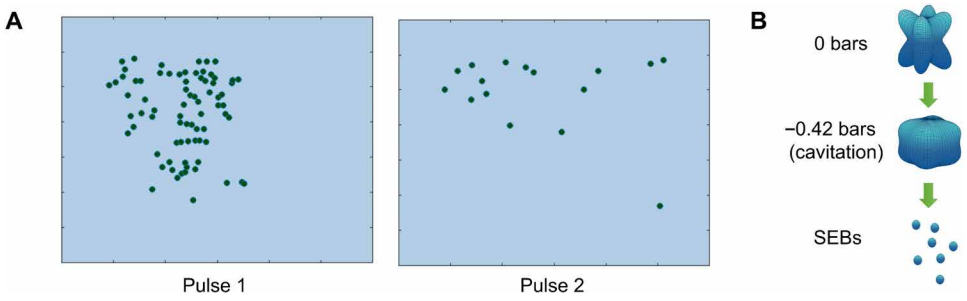

Fig. 3. Stability of FEBs after cavitation. (**A**) Snapshots for the double pulsing experiment. The number of FEBs is far higher during the first ultrasonic pulse, implying that cavitation destroys the FEBs. (**B**) Schematic of destruction of FEBs after cavitation through formation of multiple SEBs.

arrows as species A and B. The occurrence of species A of lower cavitation threshold (~140 V; see Fig. 2C) was noticeably rarer compared to species B (cavitation threshold, ~210 V). As described later, we identified the species A and B as 8EBs and 6EBs, respectively.

Example snapshots of the experimental volume are shown in the insets of Fig. 2C. The image corresponding to V_T = 250 V showed that the FEBs were positioned along a curved path, suggesting that these may correspond to quantized vortex lines on which FEBs were trapped. Few examples of photographs taken under similar conditions are shown in Fig. 2D and in section S3, where the paths were slightly different every time. The vortex lines, as expected, mostly originated below the tungsten tip where the heat input and therefore thermal counterflow were maximum. At higher V_T, the number of cavitation events increased, and it was not possible to see any definite pattern on the location of the FEBs.

Results of the experiment to investigate the stability of these objects upon cavitation are shown in Fig. 3. We applied two acoustic pulses separated by 0.5 ms, and the results (see movie S2) show a large reduction in the number of cavitation events occurring because of the second pulse. This contrasts with similar experiments performed by Guo *et al.* (*14*), who found the same SEBs to be exploded for every acoustic pulse. Our results suggest (see Fig. 3B) that the objects must be broken after the first pulse into objects with higher cavitation threshold, most likely SEBs.

To identify the two species A and B shown in Fig. 2, we needed to convert V_T into pressure wave amplitude. A possible calibration technique was to use the cavitation threshold pressure (2.12 bars) for SEBs. This required higher voltages, and beyond V_T ~ 650 V, which was lower than the SEB threshold, the ultrasound transducers broke because of large strains. To circumvent this problem, we replaced the planar transducer with a hemispherical transducer, which focused the ultrasound to achieve pressure oscillations larger than $|P_{SEB}|$ in a region of dimension of ~150 μm. The same technique has been used before to measure spinodal limit (*15*, *16*) of liquid helium, cavitation threshold of excited-state SEBs (*17*, *18*), and SEBs trapped on vortices (*18*, *19*).

Summary of more than 300 experimental measurements (details in section S4) with the hemispherical transducer is shown in Fig. 4, where the pressure axis is scaled with respect to the SEB threshold pressure, P_{SEB}. The key finding is the detection of two species of cavitation threshold at approximately 0.2 P_{SEB} and 0.3 P_{SEB}, respectively. Their ratio (~0.67) matched with the threshold voltages (140 and 210 V; ratio, ~0.67) for the species shown in Fig. 2B. The critical pressure for cavitation of multielectron bubbles (MEBs) under the

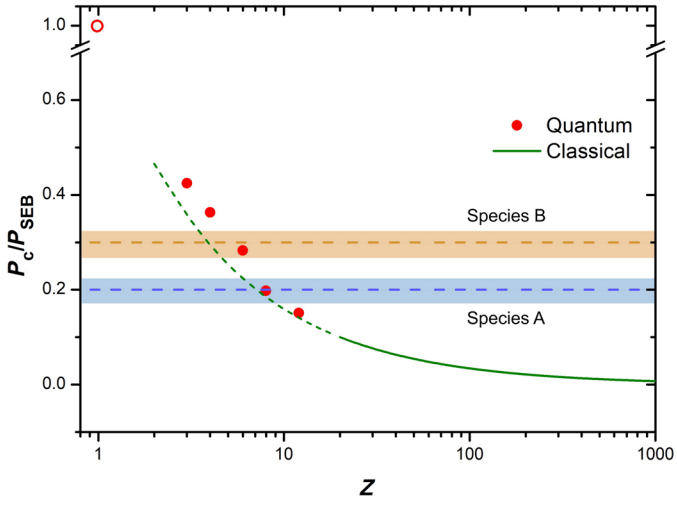

Fig. 4. Cavitation threshold of FEBs. Plot of cavitation threshold pressure P_c/P_{SEB} for bubbles containing different numbers (Z) of electrons, showing species A and B to be 8EB and 6EB, respectively. The solid green line corresponds to theoretical P_c/P_{SEB} for MEBs under classical approximation (*25*), while the solid red symbols correspond to theoretical predictions on critical pressure of FEBs including the effects due to quantum confinement.

classical (*20*) approximation (valid for $Z > 100$), where only electrostatic interactions are considered, is shown as comparison (green line). We also show results from recent calculations that included quantum confinement effects, as solid red symbols. The horizontal bands correspond to measured limits of critical pressure for the two objects A and B, and by comparing with the theoretical predictions, we identify them to be 8EBs and 6EBs, respectively.

The underlying physical mechanism to form FEBs is not trivially understood. As reported before (*21*–*23*), electrohydrodynamic instability of liquid helium surface occurs close to the capillary length $L_c \cong 0.5$ mm for critical electron densities $n_{crit} > 2 \times 10^{13}/m^2$, forming large (>200 μm below T_λ) MEBs containing more than thousand electrons. In the present experiments, we could not observe the instability of the charged surface, implying that the surface would break at length scales (λ) smaller than the experimental limit of detection. This was >5 μm in bulk liquid, which further worsens near the surface. In our experiments, surface instabilities of size $\lambda < 5$ μm resulted in various micrometer- and submicrometer-sized cavities containing multiple electrons. The stability of these MEBs and FEBs

have been debated in the past (*20*, *24*–*28*), and in this respect, our experiments provide a definite answer: These microscale objects continue to break into smaller pieces, until only two stable species of FEBs (8EBs and 6EBs) survived in large enough numbers to be detectable. Note that FEBs containing 12 electrons are also predicted to be stable against small shape fluctuations; however, we have not observed them in our experiments.

Formation of FEBs

We experimented with two types of electron sources: field emission tungsten tips and radioactive beta source (15 mCi; Ni-63 foil). For the former, high-voltage pulses were applied to a sharp tungsten tip placed (see Fig. 3A) above the liquid surface. Similar experiments on MEBs were reported (*29*, *30*) before, where the duration of the voltage pulse was ~30 to 50 ms, allowing enough time for the electrohydrodynamic instability to grow and form MEBs. In current experiments, pulse widths were too short (~0.6 ms) to form large MEBs, but instead, we detected FEBs by cavitation. We applied (see inset of Fig. 5B) voltage pulse with an amplitude of −1.2 kV and a duration of 0.2 ms to the tip, followed (variable delay) by an ultrasound drive (acoustic pulse width, 10 μs) applied to the transducer. The number of FEBs reduced as delay increased, and at long delays, SEBs could be observed (see section S5). By comparing the threshold voltages, we could identify the FEB species to be 6EBs. Even if 8EBs were present, their numbers would be significantly lower, consistent with the observations made with the planar transducer (see Fig. 2B).

One necessary condition to observe large number of FEBs was the appearance of a glow around the tip, suggesting corona discharge. The emitted light was measured by a photomultiplier tube as function of time, as shown in the top inset of Fig. 5B. The variation of cavitation probability S of the 6EBs as function of delay t_d, suggesting that FEBs were formed during the discharge (see section S1). The variation $S(t_d)$ after fitting with a double exponential suggests two relevant time scales, with the former (~130 μs) matching with the response time of the high-voltage electronics and therefore related to the rate of generation. The latter (~7 ms) is more interesting and puts a lower limit on the lifetime of the 6EBs. This is determined by either the applied electric field or flow of the normal fluid present in the experimental chamber dragging the bubbles away from the surface or alternately provides the intrinsic lifetime of the 6EBs.

The formation of the 6EBs due to the corona discharge is discussed in Materials and Methods. The large current (about microampere) during the discharge can produce very large surface electron densities, which, in turn, can break through microscopic dimples on the liquid surface and thereby carry the electrons into the liquid through SEBs and FEBs. Analogous (but opposite) cases with liquid metal ion sources (LMISs) have been observed in the past, where micro- and nanoscale droplets (*31*) were formed along with the ions injected from the tip. However, the presence of corona discharge and strong flux of electrons impinging on the surface significantly complicates the present system. The 6EBs could be observed as high as 2 K, although the experimental conditions to

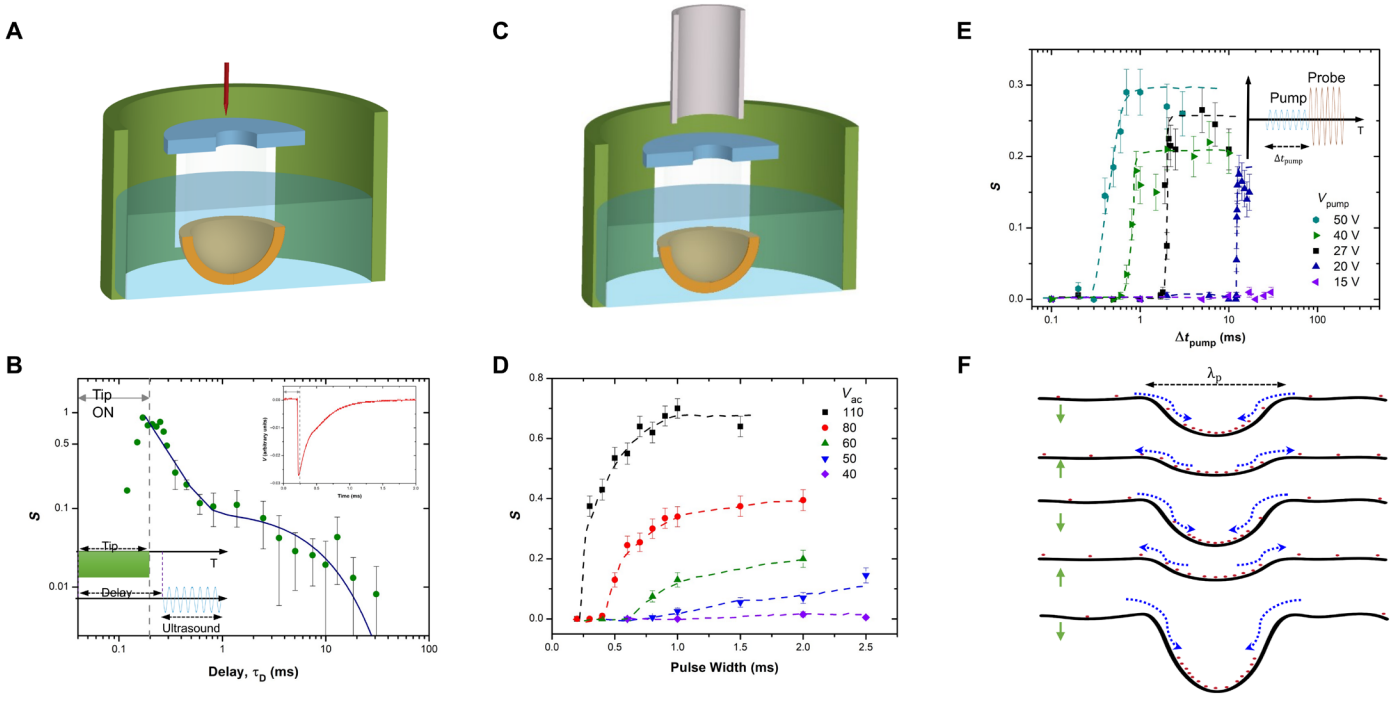

Fig. 5. Mechanism of formation of FEBs. (**A**) Schematic of the experimental setup using field emission and hemispherical transducer to form 6EBs. (**B**) Inset shows measurement of the light emitted by the tip as function of time. Also shown is the cavitation probability of the 6EBs (at V_T corresponding to P_{osc} = 0.9 bars) as a function of delay, along with a double exponential fit. (**C**) Schematic of the experimental setup using a beta source and hemispherical transducer to form 8EBs. (**D**) Probability of cavitation as function of pulse width for different values of V_T showing that a minimum duration of acoustic pulse was necessary to generate FEBs. (**E**) Cavitation probability as a function of Δt_{pump} for various V_{pump} is plotted. Inset shows schematic of the pump-probe experiment to drive the transducer at V_{pump} for duration Δt_{pump} after which a probe pulse was used to detect the FEBs. (**F**) Schematic of the proposed mechanism in which undulation of length scale λ of the charged surface couples with the applied ultrasound. The red arrows show coupling of the electrons (red circles) to the surface oscillation (green arrows).

achieve corona discharge changed because of the different vapor pressure at higher temperatures.

We performed a control experiment to check whether the impact of ultrasound with the charged surface can play a role in the generation of FEBs. The results, as shown in section S6, suggest that the presence of ultrasound was not necessary to create the FEBs if the corona discharge was present. However, as discussed next, under certain conditions, it was possible to create 8EBs using ultrasound, where either the tip or a radioactive beta source was used to create a charged helium surface.

As shown in Fig. 5C, we applied negative potential of 500 and 200 V to the source and the top ring, respectively, which ensured that the surface was charged. In this particular experiment, we used a radioactive source, so the overall densities of SEBs were lower, limited by the activity of the beta source at 5.5×10^8 primary electrons/s and electrons produced by secondary (*32*) ionization. A crucial observation in these experiments was that the FEBs were detected only when the acoustic pulse width was increased beyond 50-μs cycles. In addition, the probability increased with the pulse width. This is shown in Fig. 5D, with data shown for different values of V_T. As shown in section S7, these features were not observed for experiments with the tungsten tip, where shorter pulse widths were used. From the minimum V_T where FEBs are observed, we could detect the presence of 8EBs. Note, this does not exclude the presence of FEBs with higher critical pressure (e.g., 6EBs).

While an increase in occurrence of FEBs with acoustic pulse width can be caused by a continuous flux of FEBs entering the acoustic focus, the same cannot explain existence of a threshold in the pulse duration. We performed a control experiment (see section S8) with the hemispherical transducer placed with its axis parallel to the surface. No FEBs were detected in this configuration, which suggested the impact of ultrasound with the charged surface generated the FEBs.

To confirm this further, we designed an experiment to decouple the role of ultrasound between generation and detection of FEBs. As shown in the schematic of Fig. 5E, we drove the transducer at V_{pump} for varying duration Δt_{pump} after which a probe pulse (magnitude, 110 V; duration, 200 μs) was used to cavitate (and therefore detect) the FEBs. The choice of V_{pump} was based on two main considerations. First, beyond certain $V_T \geq 85$ V, we could observe the formation of mist, similar to experiments reported before (*33*, *34*). Note that the liquid level was present approximately 3 mm above the acoustic focus, implying distribution of acoustic radiation pressure to deform the charged surface (see section S9 for more details). Second, the 8EB threshold at −0.42 bars corresponded to $V_T = 35$ V at the hemispherical transducer. This ensured that $V_{pump} < 35$ V may be able to perturb the surface and therefore contribute toward generation of FEBs but could not induce cavitation on the FEBs present around the acoustic focus. The results shown in Fig. 3E conclusively prove that a minimum drive amplitude and duration were necessary for to produce FEBs, which were subsequently detected by the probe pulse.

The physical mechanism proposed in the model is shown in Fig. 5F and in Materials and Methods. Undulations of length λ of the liquid surface can couple with the ultrasound frequency $w_s \approx \sqrt{\sigma/(\rho\lambda^3)}$, which corresponds to deformations $\lambda \sim 0.4$ μm for the fundamental mode. The surface electrons have very high mobility (~4 $m^2/V{\cdot}s$) at 1.5 K, implying that electrons move synchronously with the surface undulations. The coupling of the electron motion with the ultrasound induced fluctuations can result in parametric instability of the charged superfluid surface, resulting in the formation of FEBs. The induced surface undulations were smaller at lower V_T, implying longer time for these few micrometer-sized instabilities to grow. Subsequently, they carry electrons into the liquid, break into smaller pieces, and lastly result in the formation of stable FEBs.

DISCUSSION

Our experiments suggest the existence of two stable species of FEBs, validated by experiments performed with different ultrasound transducer geometries and electron sources. The formation of 6EBs was more abundant with the tip (corona discharge) experiments, while the 8EBs were readily formed by ultrasound induced parametric instability of the surface, where the surface was charged by either the tip or the radioactive source. This difference was probably due to different initial conditions in which they were generated and merits further theoretical investigation. The nonobservation of objects with lower cavitation threshold suggests that electron bubbles with higher number of electrons are unstable against small fluctuations or their number density is immeasurably low. Note that the FEBs trapped on vortex lines will remove kinetic energy from the superfluid, which will reduce the magnitude of their cavitation threshold. This difference is expected to be less than 2% for 6EBs and 8EBs and therefore not considered. However, entrapment on vortices can provide further stabilizing effects, due to the (negative) Bernoulli pressure (*20*) acting on the bubbles. Last, it is interesting to ask whether FEBs have been observed in previous experiments. The requirement of a charged surface to observe these objects and their decoration along vortex lines excludes phenomena such as cavitation due to Penning ionization of dimers (*35*, *36*) or deposition of energy due to high-energy primary electrons (*37*). Of relevance are the 13 species of exotic ions (*38*, *39*), which are negative-charged objects observed under similar discharge conditions that moved faster than SEBs. The structure of exotic ions is not yet settled (*40*), and FEBs could be a likely candidate. In the future, measurement of cavitation threshold and, therefore, size of the exotic ions and/or estimating the mobility of the FEBs can provide a definite answer to this question.

Thomson problem is relevant to many problems of practical significance ranging from structures of viruses (*41*, *42*) and other supramolecular assemblies, to arrangement of colloidal (*43*, *44*) particles and aerosols in confined (*45*) spaces. The novel nanomaterial reported here simultaneously incorporates soft and quantum effects to the Thomason problem. The decoration of quantized vortex lines by FEBs could provide a simpler experimental platform in imaging quantum turbulence (*46*) due to the ease of continuous generation and easier observation, which can be advantageous over visualization techniques based on SEBs (*14*) and hydrogen crystallites (*47*). We believe that FEBs could be particularly useful as few body quantum simulators, incorporating both charge and spin (*48*) interactions. It may be possible to store the FEBs in a radio-frequency (RF) Paul trap, similar to previous studies (*30*, *49*) with MEBs, and to investigate them over an extended duration.

MATERIALS AND METHODS

Electronics and imaging system for the cavitation experiments

To drive the piezoelectric transducer hemispherical or planar transducer with a resonance frequency of 1 MHz, we used a RITEC Gated RF amplifier (GA 2500A). The duty cycle of the instrument is

0.1%, but the maximum pulse width that can be obtained is 200 μs, limited by the hardware. To amplify longer pulse widths, we have used Thorlabs HVA 200, which could provide pulse durations longer than 10 ms, with the maximum amplitude of 80 V. In the imaging setup, light-emitting diode (LED) array or collimated high-power LED was used for the illumination. We installed a 100-mm convex lens at the 4-K radiation shield whose focal plane was at the center of the experimental chamber. To collect the light, an infinity corrected tube lens (Edmond MT1) with a focal length of 200 mm was used near the 300-K window. The combination of the convex lens and the tube lens helped in focusing the central plane of the chamber at the imaging sensor. The magnification of this optical system was ×2 . We have used either Photron SA4 or Mini Cam for recording the high-speed videos. The frames per second varied from 10,000 to 225,000 fps depending on the experimental requirements. For cavitation measurements, we only consider events in the bulk and not events that occur very close to the surface of the liquid or the ultrasonic transducer.

Generation of FEBs with the tungsten tip

The typical voltages applied to the tip (amplified using Trek amplifiers), placed in helium vapor above the liquid surface, were in the range of −1.2 to −1.8 kV for 0.2 to 0.6 ms. Both SEBs and FEBs were detected only when a red/orange discharge was observed. A minimum amplitude and width of the voltage pulse were necessary to observe the discharge, which, in turn, were functions of temperature. We believe that the large current (about microampere) emitted by the tip during the discharge was responsible for the injection of electrons in the form of SEBs and FEBs into the liquid. While direct injection of electrons with energy higher than 1 eV in the form of SEBs is conceivable, the formation of FEBs through the same mechanism would require much larger number of electrons reaching the same region of the surface concurrently. To estimate the relevant parameters, we consider a current I concentrated over a circular region of radius L. The surface density (n_s) of electrons could be estimated by equating the incoming rate of electrons against the surface current, which, in turn, is determined by the surface electron mobility (μ_s) and space charge–limited electric field (E_s) parallel to the liquid surface, given by: $\frac{I}{\pi L^2} = n_s e \mu_s E_s$. Accordingly, one estimates the surface density $n_s = \sqrt{\frac{2I\varepsilon_0}{\mu_s e^2 \pi L^3}}$ to be ~2×10^{14}/m^2 for typical experimental parameters, I = 1 μA and L = 1 mm. At this large n_s, macroscale electrohydrodynamic instabilities are expected to form but over much longer time scales (>30 ms). On the other hand, one may consider a microscopic undulation of length λ, which could become unstable when the electronic pressure ($\frac{n_s^2 e^2}{\varepsilon_0}$) exceeds the pressure ($\frac{2\sigma}{\lambda}$) due to the surface tension. Accordingly, one can estimate a typical instability length $\lambda = \frac{\mu_s \sigma \pi L^3}{I} \sim 4$ μm for typical experimental parameters. In addition, relevant to this phenomenon, for ion injection from LMISs, additional microscale and nanoscale droplets can get injected from multiple locations, including back end of the Taylor-Gilbert cone. It is possible that analogous phenomena can further contribute to the direct injection process of the FEBs described here.

Ultrasound-induced generation of FEBs

We describe a simple model to understand how the impact of ultrasound with the charged surface can lead to generation of FEBs. The equation of motion of the surface modes u_k could be expressed as $\frac{d^2 u_k}{dt^2} + \omega^2(t)\, u_k = 0$, where the role of ultrasound was to modify the mode frequency $\omega^2(t) = \omega_0^2(1 + h\cos\omega_s t)$. Here, w_s is the angular frequency corresponding to the ultrasound at 1 MHz, and $\omega_0^2 h$ corresponds to coupling of the ultrasound with charged surface waves. We express the frequency of the uncoupled mode $\omega_0^2 = gk + \frac{\sigma k^3}{\rho}[1 + \xi^2 k^2]^{-1/2} - \frac{e^2 n_e^2}{\varepsilon\rho} k^2$, where ρ is the density of liquid helium, ε is the dielectric constant of the liquid, ξ is the large (*50*) surface displacement induced by the ultrasound, n_e is the surface density of electrons, and e is the charge of an electron. The coupling of the charged surface with ultrasound was expressed as $\omega_0^2 h = \frac{n_e^2 e^2 k^2}{\varepsilon\rho} f_c$. The important limits of this model were the surface electron density to be less than the critical density ($n_e < n_{crit}$) and the electron-ripplon-ultrasound coupling term $f_c \leq 1$, signifying that local densities cannot exceed much more than n_{crit}.

The physical mechanism proposed in the model is shown in Fig. 3F. Undulations of length λ of the liquid surface can couple with the ultrasound frequency $w_s \approx \sqrt{\sigma/(\rho\lambda^3)}$, which corresponds to deformations λ ~ 0.4 μm for the fundamental mode. The surface electrons have very high mobility (~4 m^2/V·s) at 1.5 K, implying that electrons move synchronously with the surface undulations. The parameter ξ varied linearly with the transducer voltage, which could be estimated from the threshold of mist formation, corresponding to $\xi_{max} = 0.73\,\lambda_s$ at V_T = 85 V. Here, λ_s = 230 μm is the wavelength of the ultrasound. The strongest parametric resonance occurs for wave vector k_p at which $\omega_s^2 = 4w_0^2(\xi, n_e, k_p)$, corresponding to an instability length scale $\lambda_p = \frac{2\pi}{k_p} \approx \sqrt{\frac{\sigma}{\xi\rho}}\frac{8\pi}{w_s}$, was determined primarily by the ξ term and only slightly affected by the magnitude of n_e. We propose that these microscopic instabilities (λ_p ~ few micrometers) carry electrons into the liquid, possibly break into smaller pieces, and lastly result in the formation of stable FEBs. These would further move under the action of applied fields or can get trapped on vortex lines.

The physically permissible highest value of $h = \frac{n_e^2 e^2 k^2}{\varepsilon\rho\omega_0^2} f_c = 3 \times 10^{-3}$ occurs at $f_c = 1$, $k = k_p$ ($\lambda_p \approx 3.5$ μm) and $n_e = n_{crit}$. Under the conditions $h \ll 1$, we can estimate the growth time (*51*) of the instabilities as $\tau^{-1} = \frac{h\omega_0}{4} = \frac{e^2 n_e^2 k^2}{4\varepsilon\omega_0\rho} f_c$ assuming no dissipation. The growth, as expected is slower for smaller surface undulations and lower magnitude of the electron-ripplon-ultrasound coupling. The corresponding experimental parameters were identified as the threshold duration Δt_{pump} of the pump pulse of amplitude V_{pump} at which FEBs were generated, also shown in fig. S9. The experimental and theoretical results were comparable for $f_c < 1$, which was consistent with the physical picture presented here. The coupling term f_c increased with higher ξ, which is also reasonable considering that more electrons would flow in and out of larger surface undulations. The occurrence of FEBs varied with the level of the liquid present in the experimental chamber in scale of the sound wavelength λ_s, and this was reasonable considering that the surface undulations were strong function of the ultrasound drive.

SUPPLEMENTARY MATERIALS

Supplementary material for this article is available at http://advances.sciencemag.org/cgi/content/full/7/28/eabi7128/DC1

REFERENCES AND NOTES

1. G. M. Whitesides, B. Grzybowski, Self-assembly at all scales. *Science* **295**, 2418–2421 (2002).

2. Y. Pennec, W. Auwärter, A. Schiffrin, A. Weber-Bargioni, A. Riemann, J. V. Barth, Supramolecular gratings for tuneable confinement of electrons on metal surfaces. *Nat. Nanotechnol.* **2**, 99–103 (2007).
3. B. N. Taber, C. F. Gervasi, J. M. Mills, D. A. Kislitsyn, E. R. Darzi, W. G. Crowley, R. Jasti, G. V. Nazin, Quantum confinement of surface electrons by molecular nanohoop corrals. *J. Phys. Chem. Lett.* **7**, 3073–3077 (2016).
4. Q. Li, R. Cao, H. Ding, Quantum size effect in nanocorrals: From fundamental to potential applications. *Appl. Phys. Lett.* **117**, 060501 (2020).
5. P. Leiderer, Electrons at the surface of quantum systems. *J. Low Temp. Phys.* **87**, 247–278 (1992).
6. H. J. Maris, Electrons in liquid helium. *J. Phys. Soc. Jpn.* **77**, 111008 (2008).
7. A. Fetter, *The Physics of Liquid and Solid Helium* (Wiley, 1976), vol. 1.
8. J. J. Thomson, XXIV. On the structure of the atom: An investigation of the stability and periods of oscillation of a number of corpuscles arranged at equal intervals around the circumference of a circle; with application of the results to the theory of atomic structure. *London Edinburgh Dublin Philos. Mag. J. Sci.* **7**, 237–265 (1904).
9. L. Yang, Z. Yao, Two and three electrons on a sphere: A generalized Thomson problem. *Phys. Rev. B.* **97**, 235431 (2018).
10. W. Wei, Z. Xie, H. J. Maris, Electron bubbles in liquid ^{4}He containing a small number of electrons. *Phys. Rev. B* **89**, 064504 (2014).
11. Y. Xing, H. J. Maris, Properties of few-electron bubbles in superfluid Helium-4. *J. Low Temp. Phys.* **202**, 399–409 (2021).
12. K. W.-K. Shung, F.-L. Lin, Structure of multielectron bubbles in liquid helium. *Phys. Rev. B.* **45**, 7491–7494 (1992).
13. N. Yadav, V. Vadakkumbatt, H. J. Maris, A. Ghosh, Exploding and imaging of electron bubbles in liquid helium. *J. Low Temp. Phys.* **187**, 618–626 (2017).
14. W. Guo, D. Jin, G. M. Seidel, H. J. Maris, Experiments with single electrons in liquid helium. *Phys. Rev. B.* **79**, 054515 (2009).
15. F. Caupin, S. Balibar, Cavitation pressure in liquid helium. *Phys. Rev. B* **64**, 064507 (2001).
16. J. A. Nissen, E. Bodegom, L. C. Brodie, J. S. Semura, Tensile strength of liquid ^{4}He. *Phys. Rev. B.* **40**, 6617–6624 (1989).
17. D. Konstantinov, H. J. Maris, Detection of excited-state electron bubbles in superfluid helium. *Phys. Rev. Lett.* **90**, 025302 (2003).
18. A. Ghosh, H. J. Maris, Observation of a new type of electron bubble in superfluid helium. *Phys. Rev. Lett.* **95**, 265301 (2005).
19. J. Classen, C.-K. Su, M. Mohazzab, H. J. Maris, Electrons and cavitation in liquid helium. *Phys. Rev. B.* **57**, 3000–3010 (1998).
20. W. Guo, D. Jin, H. J. Maris, Stability of multielectron bubbles in liquid helium. *Phys. Rev. B* **78**, 014511 (2008).
21. A. P. Volodin, M. S. Khaĭkin, V. S. Édel'man, Development of instability and bubblon production on charged surface of helium. *J. Exp. Theor. Phys.* **26**, 543 (1977).
22. U. Albrecht, P. Leiderer, Multielectron bubbles in liquid helium. *Europhys. Lett.* **3**, 705–710 (1987).
23. N. Yadav, P. K. Rath, Z. Xie, Y. Huang, A. Ghosh, Multielectron bubbles in liquid helium. *J. Low Temp. Phys.* **201**, 658–675 (2020).
24. V. B. Shikin, Multielectron bubbles in liquid helium. *JETP Lett.* **27**, (1978).
25. M. M. Salomaa, G. A. Williams, Electronic structure of multielectron bubbles in liquid helium. *Phys. Scr.* **T4**, 204–207 (1983).
26. I. F. Silvera, J. Blanchfield, J. Tempere, Stability of multielectron bubbles against single-electron split-off. *Phys. Status Solidi Basic Res.* **237**, 274–279 (2003).
27. J. Tempere, I. F. Silvera, J. T. Devreese, Effect of pressure on statics, dynamics, and stability of multielectron bubbles. *Phys. Rev. Lett.* **87**, 275301 (2001).
28. M. M. Salomaa, G. A. Williams, Structure and stability of multielectron bubbles in liquid helium. *Phys. Rev. Lett.* **47**, 1730–1733 (1981).
29. E. M. Joseph, V. Vadakkumbatt, A. Pal, A. Ghosh, High speed imaging of generation and collapse of multielectron bubbles in liquid helium. *J. Low Temp. Phys.* **175**, 78–84 (2014).
30. V. Vadakkumbatt, E. Joseph, A. Pal, A. Ghosh, Studying electrons on curved surfaces by trapping and manipulating multielectron bubbles in liquid helium. *Nat. Commun.* **5**, 4571 (2014).
31. R. G. Forbes, Understanding how the liquid-metal ion source works. *Vacuum* **48**, 85–97 (1997).
32. G. M. Seidel, T. M. Ito, A. Ghosh, B. Sethumadhavan, Charge distribution about an ionizing electron track in liquid helium. *Phys. Rev. C* **89**, 25808 (2014).
33. H. Kim, K. Seo, B. Tabbert, G. A. Williams, Properties of superfluid fog produced by an ultrasonic transducer. *J. Low Temp. Phys.* **121**, 621–626 (2000).
34. H. Kim, K. Seo, B. Tabbert, G. A. Williams, Properties of superfluid fog. *Europhys. Lett.* **58**, 395–400 (2002).
35. N. Yadav, V. Vadakkumbatt, A. Ghosh, Observation of cavitation on electron bubbles at small negative pressures. *J. Low Temp. Phys.* **201**, 97–105 (2020).
36. A. Ghosh, H. Maris, Cavitation in superfluid helium possibly arising from Penning ionization of dimers. *J. Low Temp. Phys.* **134**, 251–256 (2004).
37. Y. Yang, S. Sirisky, W. Wei, G. M. Seidel, H. J. Maris, Nucleation of bubbles by electrons in liquid helium-4. *J. Low Temp. Phys.* **192**, 48–64 (2018).
38. G. G. Ihas, T. M. Sanders Jr., Exotic negative carriers in liquid helium. *Phys. Rev. Lett.* **27**, 383–386 (1971).
39. V. L. Eden, P. V. E. McClintock, The effect of strong electric fields on exotic negative ions in He II: Possible evidence for the nucleation of charged vortex rings. *Phys. Lett. A.* **102**, 197–200 (1984).
40. Y. Xing, H. J. Maris, Electrons and exotic ions in superfluid helium-4. *J. Low Temp. Phys.* **201**, 634–657 (2020).
41. C. J. Marzec, L. A. Day, Pattern formation in icosahedral virus capsids: The papova viruses and Nudaurelia capensis beta virus. *Biophys. J.* **65**, 2559–2577 (1993).
42. R. Zandi, D. Reguera, R. F. Bruinsma, W. M. Gelbart, J. Rudnick, Origin of icosahedral symmetry in viruses. *Proc. Natl. Acad. Sci. U.S.A.* **101**, 15556–15560 (2004).
43. W. T. M. Irvine, V. Vitelli, P. M. Chaikin, Pleats in crystals on curved surfaces. *Nature* **468**, 947–951 (2010).
44. P. Lipowsky, M. J. Bowick, J. H. Meinke, D. R. Nelson, A. R. Bausch, Direct visualization of dislocation dynamics in grain-boundary scars. *Nat. Mater.* **4**, 407–411 (2005).
45. H. Kusumaatmaja, D. J. Wales, Defect motifs for constant mean curvature surfaces. *Phys. Rev. Lett.* **110**, 165502 (2013).
46. W. F. Vinen, J. J. Niemela, Quantum turbulence. *J. Low Temp. Phys.* **128**, 167–231 (2002).
47. G. P. Bewley, D. P. Lathrop, K. R. Sreenivasan, Superfluid helium: Visualization of quantized vortices. *Nature* **441**, 588 (2006).
48. L. Lehtovaara, J. Eloranta, Small multielectron bubbles in bulk superfluid ^{4}He, in *AIP Conference Proceedings* (American Institute of Physics, 2006), pp. 167–168.
49. D. K. Pradhan, N. Yadav, P. K. Rath, A. Ghosh, Trapping multielectron bubbles using a point Paul trap. *J. Low Temp. Phys.* , 1–8 (2021).
50. G. D. Crapper, An exact solution for progressive capillary waves of arbitrary amplitude. *J. Fluid Mech.* **2**, 532–540 (1957).
51. L. Landau, E. Lifshitz, *Mechanics: Volume 1* (Butterworth-Heinemann, ed. 1, 1976), vol. 1.

Acknowledgments: We thank A. Ghosh, E. Joseph, H. Maris, J. Jain, and V. Vadakkumbatt for helpful discussions. **Funding:** We thank SERB-HRHR and MHRD-SPARC for funding this research. We also acknowledge funding from MHRD, MeitY, and DST Nano Mission for supporting the facilities at CeNSE. **Author contributions:** N.Y. and A.G. designed the experiments together. N.Y. performed the experiments and analyzed the experimental data. A.G. and P.S. developed the theoretical model. A.G. supervised the research and wrote the manuscript. **Competing interests:** The authors declare that they have no competing interests. **Data and materials availability:** All data needed to evaluate the conclusions in the paper are present in the paper and/or the Supplementary Materials. Additional data related to this paper may be requested from the authors.

Submitted 25 March 2021
Accepted 26 May 2021
Published 9 July 2021
10.1126/sciadv.abi7128

Citation: N. Yadav, P. Sen, A. Ghosh, Bubbles in superfluid helium containing six and eight electrons: Soft, quantum nanomaterial. *Sci. Adv.* **7**, eabi7128 (2021).

ScienceAdvances

Bubbles in superfluid helium containing six and eight electrons: Soft, quantum nanomaterial

Neha YadavProsenjit SenAmbarish Ghosh

Sci. Adv., 7 (28), eabi7128.

Science Advances (ISSN 2375-2548) is published by the American Association for the Advancement of Science. 1200 New York Avenue NW, Washington, DC 20005. The title *Science Advances* is a registered trademark of AAAS.